Universidade de São Paulo
Instituto de Astronomia, Geofísica e Ciências Atmosféricas
Departamento de Astronomia

Laura Fernanda do Amarante Luque

# Exoplanets: Comparative Anatomy of Atmospheres

São Paulo
2025

Laura Fernanda do Amarante Luque

# Exoplanets: Comparative Anatomy of Atmospheres

Trabalho de Conclusão de Curso apresentado ao Departamento de Astronomia do Instituto de Astronomia, Geofísica e Ciências Atmosféricas da Universidade de São Paulo como requisito parcial para a obtenção do título de Bacharel em Astronomia.

Vertente: Pesquisa Básica
Orientador: Prof. Dr. Eduardo Janot Pacheco

São Paulo
2025

*Dedico este trabalho a minha mãe, Cristina Fernandes do Amarante, e ao meu pai, José Luis Fernando Luque Alejos, que sempre me apoiaram e me incentivaram a seguir meus sonhos.*

# Agradecimentos

Aos meus pais, principalmente, pelo amor incondicional que ajudou a formar a pessoa que sou hoje. Obrigada por sempre me acompanharem nessa jornada e por darem todo o apoio necessário para que eu pudesse concluir minha graduação fora do Rio. Espero poder retribuir essa dedicação sendo um orgulho para vocês.

À minha irmã, Luisa Helena do Amarante Luque, por quem tenho muito carinho, por fazer parte da minha vida.

Ao meu orientador, Eduardo Janot Pacheco, pelos grandes ensinamentos, pela motivação e por me guiar durante essa jornada.

A todos os professores que conheci durante a minha graduação, por me transmitirem o conhecimento.

Ao meu amigo Carlos, que esteve ao meu lado desde o primeiro dia da faculdade, nos bons e nos maus momentos. Te agradeço pelo apoio, pela compreensão e pelo carinho que você sempre demonstrou. Sem você, esses quatro anos teriam sido muito mais difíceis.

Aos meus amigos, Thayná, João, Hércules, Luana e a todo o grupo do Besouro, por tornarem minha graduação muito mais divertida. Obrigada pelas risadas, pelos trabalhos em grupo e pela companhia.

Aos meus queridos cachorros, Martin e Marie, que são minhas estrelas.

À FAPESP e ao PUB, pelo apoio financeiro, sob o projeto n$^o$: 2023/10700-1.

Ao Instituto de Astronomia, Geofísica e Ciências Atmosféricas (IAG/USP), por proporcionar todo o ambiente e a infraestrutura necessários para realizar meu sonho de ser astrônoma.

---

Esta tese/dissertação foi escrita em LaTeX com a classe IAGTESE, para teses e dissertações do IAG.

"*A astronomia é uma experiência de humildade e formação de caráter.*"

Carl Sagan

"*Nada é mais belo do que o mistério do universo revelando-se à razão humana.*"

Maria Mitchell

# Abstract

With the large number of currently known exoplanets, characterizing their atmospheres at a population level is becoming possible. Knowing the atmospheres of planets in other systems can help us understand the extent to which the Solar System is unique or common, as well as issues related to planetary formation and evolution and the habitability of exoplanets. In this work, we compare the atmospheric properties (composition and abundances) of a sample of exoplanets with the Solar System. The sample of exoplanets was chosen by selecting only the exoplanets observed by the JWST and includes 24 hot Jupiters, 12 sub-Neptunes and 20 rocky planets. In addition, we calculate the habitable zone and the tidal locking radius for the systems in the sample. Combining these results with the comparative analysis of atmospheres, a list of priority targets is selected for future missions. The comparative analysis of molecular abundances in hot Jupiters relative to Jupiter and Saturn indicates generally lower $H_2O$ abundances but consistently higher $CO_2$ and $CO$ abundances in the exoplanets, reflecting the intensification of photochemical processes in hot Jupiters. The atmospheres of sub-Neptunes appear to share characteristics with both rocky planets and Neptune, demonstrating the diversity of this class of planet. Data on rocky planets, on the other hand, are insufficient, highlighting that the study of small planet atmospheres remains a challenge. Of the planets in the sample, LHS 1140 b, K2-18 b and HD 80606 b are in the habitable zone, but they are tidally locked. The only planet that has not yet assumed a synchronous orbit is the hot Jupiter HIP 67522 b, but it is likely to do so in $\sim 0.08\ Gyr$. In addition to other reasons, because LHS 1140 b potentially has an atmosphere similar to Earth's, K2-18 b has been the target of biosignature detection and HD 80606 b may host habitable exomoons, we have selected these planets as priority targets for future missions.

# List of Figures

4.1 The ratios between the abundance in the exoplanet and in Jupiter, as a function of orbital period. Green dots are $H_2O$ abundance, red dots are $CO_2$ and blue dots are $CO$. The figure indicates that $CO_2$ and $CO$ are significantly enhanced in hot Jupiters when compared to Jupiter, while water is commonly less abundant. . . . . 32

5.1 Stellar mass as a function of tidal locking radius for times 0.1 Gyr (dotted line), 1 Gyr (dashed line) and 10 Gyr (solid line). The color map indicates the age of the exoplanets in the sample, which are represented by dots. The only planet that is possibly not tidally locked is circled. . . . . 39

# List of Tables

2.1 Atmospheric compositions of Solar System planets . . . . . 19

4.1 Comparison of molecular abundances between hot Jupiters and the Solar System . . . . . 29

4.2 Comparison of molecular abundances between sub-Neptunes, rocky exoplanets and the Solar System . . . . . 34

5.1 Habitable zone boundaries. . . . . 36

A.1 Planetary properties and atmospheric detections for 24 hot Jupiters . . . . 52

A.2 Planetary properties and atmospheric detections for rocky exoplanets . . . 53

A.3 Planetary properties and atmospheric detections for sub-Neptunes . . . . . 54

# Contents

*1. Introduction* . . . . . 17

*2. The Solar System Atmospheres* . . . . . 19

2.1 Venus . . . . . 19

2.2 Earth . . . . . 21

2.3 Mars . . . . . 22

2.4 Jupiter and Saturn . . . . . 23

2.5 Neptune . . . . . 23

*3. Exoplanet Atmospheres* . . . . . 25

3.1 Hot Jupiters . . . . . 25

3.2 Rocky planets and Sub-Neptunes . . . . . 27

*4. Comparative Analysis* . . . . . 29

*5. Habitable Zone and Tidal Locking Radius* . . . . . 35

*6. Conclusions* . . . . . 41

*Bibliography* . . . . . 43

*Appendix* 49

*A. Sample of this Work: Atmospheres and References* . . . . . 51

Chapter 1

# Introduction

Since the discovery of the first exoplanet orbiting a main sequence star in 1995, by Mayor and Queloz (1995), the detection of exoplanets has increased rapidly. To date, there are more than 5900 confirmed exoplanets, according to NASA's exoplanet archive. The characterization of exoplanets on a population level opens up new frontiers for the comprehension of planetary formation and evolution, as well as for studying habitability and the search for life beyond Earth. Furthermore, characterizing exoplanets is a powerful tool for studying the Solar System itself, as observing how other planetary systems in the Galaxy are configured can reveal possible trends and mechanisms of planetary formation and habitability.

An essential part of characterizing exoplanets is observing their atmospheres. For transiting planets, the most used method is transmission spectroscopy. In this case, the planet's transmission spectrum is obtained during primary transit, when the planet passes in front of the host star. It reveals the atmospheric composition and can also indicate the presence and composition of aerosols (like clouds and haze). On the other hand, secondary transit (when the planet passes behind the star) reveals the planet's thermal emission, which can indicate the absence (or presence) of an atmosphere, cloud properties, atmospheric composition and average temperature (Kempton and Knutson, 2024). The atmosphere of an exoplanet can be studied to assess the correlation between planetary formation and the different types of atmospheres (Howell, 2020). In addition, observing atmospheres allows for the remote detection of biosignatures. On Earth, for example, most signs of life are found in the atmosphere, as certain gases are released by metabolic processes and some chemical imbalances are caused by life (Krissansen-Totton et al., 2016; Wordsworth and Kreidberg, 2022). Currently, thanks to the launch of the JWST (James

Webb Space Telescope) and the future launch of other telescopes designed specifically to detect and characterize exoplanets, such as ARIEL (Atmospheric Remote-sensing Infrared Exoplanet Large-survey), scheduled for launch in 2029, and PLATO (Planetary Transits and Oscillations of Stars), to be launched in 2026 (Rauer et al., 2014; Tinetti et al., 2018), the characterization of several exoplanet atmospheres is becoming possible. In particular, the characterization of small planet atmospheres is expected to improve with JWST observations, due to its larger diameter and infrared wavelength range compared to previous telescopes.

In this work, results on exoplanet atmospheres from the literature have been compiled for comparison with those of the Solar System. The analysis is carried out on a sample of exoplanets comprising 24 hot gas giants (hot Jupiters), 12 sub-Neptunes and 20 rocky planets. This sample was chosen by selecting only the exoplanets observed by the JWST. In addition, we aim to calculate the habitable zone and the tidal locking radius for each system in the sample. Combining these results with the comparative analysis of atmospheres, a list of priority targets is selected for future missions focused on exoplanets. Chapter 2 describes the atmospheres of the Solar System's planets, including those of the rocky planets Venus, Earth and Mars, as well as the gaseous planets Jupiter, Saturn and Neptune. Chapter 3 discusses the exoplanets, presenting the information collected on the atmospheres of hot Jupiters, terrestrial exoplanets and sub-Neptunes. Chapter 4 refers to the comparative analysis between the atmospheres of the exoplanets and the Solar System. Chapter 5 presents the results on habitable zone and tidal locking radius calculations. Finally, we select the priority targets and conclude in Chapter 6.

Chapter 2

# The Solar System Atmospheres

This work will consider the atmospheres of six planets in the Solar System: Venus, Earth, Mars, Jupiter, Saturn and Neptune. The atmospheres of rocky exoplanets will be compared to those of Venus, Earth and Mars. Hot Jupiters will be compared to the atmospheres of Jupiter and Saturn. Meanwhile, sub-Neptunes are compared to the rocky planets and Neptune, as this class of exoplanets is of unknown nature and may be similar to either a Neptune-like or an Earth-like planet. To do this, we consider composition (molecules and other species) and the abundance of these species. Table 2.1 shows these atmospheric features for the Solar System's planets.

*Table 2.1* - Atmospheric compositions of Solar System planets

| Atmospheric Properties | Venus | | Earth | | Mars | | Jupiter | | Saturn | | Neptune | |
|---|---|---|---|---|---|---|---|---|---|---|---|---|
| Molecules\|Abundances | $CO_2$ | $9.6 \times 10^{-1}$ | $N_2$ | $7.8 \times 10^{-1}$ | $CO_2$ | $9.5 \times 10^{-1}$ | $H_2$ | $8.6 \times 10^{-1}$ | $H_2$ | $(7.3-8) \times 10^{-1}$ | $H_2$ | $8.0 \times 10^{-1}$ |
| | $N_2$ | $3.5 \times 10^{-2}$ | $O_2$ | $2.1 \times 10^{-1}$ | $N_2$ | $2.8 \times 10^{-2}$ | He | $1.4 \times 10^{-1}$ | He | $(1.8-2.5) \times 10^{-1}$ | He | $1.9 \times 10^{-1}$ |
| | $SO_2$ | $1.5 \times 10^{-4}$ | Ar | $9.3 \times 10^{-3}$ | Ar | $2.0 \times 10^{-2}$ | $H_2O$ | $(2.5^{2.2}_{1.6}) \times 10^{-3}$ | $H_2O$ | $\sim 10^{-3}$ | $CH_4$ | $1.5 \times 10^{-2}$ |
| | Ar | $7.0 \times 10^{-5}$ | $H_2O$ | $(0-4) \times 10^{-2}$ | $O_2$ | $1.4 \times 10^{-3}$ | $CH_4$ | $1.8 \times 10^{-3}$ | $CH_4$ | $(4.5^{2.5}_{1.9}) \times 10^{-3}$ | $C_2H_6$ | $8.5 \times 10^{-7}$ |
| | CO | $4.0 \times 10^{-5}$ | $CO_2$ | $4.1 \times 10^{-4}$ | CO | $6.0 \times 10^{-4}$ | $NH_3$ | $7 \times 10^{-4}$ | $NH_3$ | $\sim 6 \times 10^{-4}$ | $C_2H_2$ | $3.3 \times 10^{-8}$ |
| | $H_2O$ | $3.0 \times 10^{-5}$ | Ne | $1.8 \times 10^{-5}$ | $H_2O$ | $3.0 \times 10^{-4}$ | $H_2S$ | $7.7 \times 10^{-5}$ | $PH_3$ | $(7.0^{3.0}_{2.0}) \times 10^{-6}$ | CO | $1.1 \times 10^{-6}$ |
| | Ne | $5.0 \times 10^{-6}$ | $CH_4$ | $1.8 \times 10^{-6}$ | Ne | $2.5 \times 10^{-6}$ | $C_2H_6$ | $(1-5) \times 10^{-6}$ | $C_2H_6$ | $(3 \pm 1) \times 10^{-6}$ | $H_2O$ | $2 \times 10^{-9}$ |
| | | | | | | | $C_2H_2$ | $(3-10) \times 10^{-8}$ | $C_2H_2$ | $(2.1 \pm 1.4) \times 10^{-7}$ | $H_2S$ | $\sim 10^{-7}$ |
| | | | | | | | $CO_2$ | $4 \times 10^{-10}$ | $H_2S$ | $< 2 \times 10^{-7}$ | | |
| | | | | | | | CO | $7.5 \times 10^{-10}$ | CO | $(1 \pm 0.3) \times 10^{-9}$ | | |
| | | | | | | | | | $CO_2$ | $3 \times 10^{-10}$ | | |

## *2.1 Venus*

Venus has the densest atmosphere among the terrestrial planets of the Solar System. When observed from afar, it can appear similar to Earth due to its similar size and mass.

However, Venus differs greatly from Earth, especially when it comes to its atmosphere. Venus' atmosphere is composed of 96.5% $CO_2$, 3.5% $N_2$ and other trace gases. Moreover, the surface is completely covered by a thick layer of sulfuric acid clouds (Kane et al., 2019). The $CO_2$-dominated atmosphere is probably due to the absence of oceans, which prevents the carbon from being removed from the air and trapped in sediment rock, as occurs on Earth (Ingersoll, 1969). The excess of $CO_2$ results in a runaway greenhouse effect that raises the surface average temperature to 750 K, making Venus the most hostile environment among the Solar System's inner planets. Besides that, Venus' atmosphere is dense enough to cause a high surface pressure 92 times greater than Earth's (Walker, 1975; Kane et al., 2019). In fact, these differences raise the question of why Venus ended up in such extreme conditions, while Earth is still habitable.

It is claimed that Venus and Earth were formed from the same material that made up the protoplanetary disk. Some research (Way et al., 2016) that used climate change models concluded that Venus might have had oceans of water in its past. In this scenario, the most plausible explanation for the water loss on Venus is the runaway greenhouse effect (Walker, 1975). Although the atmospheres of Earth and Venus were composed of the same material when the Solar System formed, it is clear that these planets followed different evolution paths. The runaway greenhouse effect might have been caused by the planet's extra proximity to the Sun (Walker, 1975; Kane et al., 2019). The extra solar flux made the early Venus' oceans evaporate, which caused the liquid water on the surface to turn into water vapor in the atmosphere. Because water vapor is a great absorber of infrared wavelengths (like carbon dioxide), its accumulation in the atmosphere increased the infrared opacity and intensified the greenhouse effect. Despite that, there is currently a low abundance of water vapor in the Venusian atmosphere. The possible reasons for that are hydrogen escaping to space and the consumption of the remaining oxygen by oxidizable material on the surface. There is also the possibility of oxygen combining with hydrocarbons in the atmosphere to form carbon dioxide. Thus, the shorter distance between Venus and the Sun might be what caused this divergent atmospheric evolution (Kane et al., 2019).

## 2.2 Earth

Earth is the only inhabited planet in the Solar System and also the only currently known habitable world in the Universe, which makes its atmosphere the only solid reference we have for an atmosphere that can shelter life and exhibit biosignatures. As Earth's atmosphere can be directly observed, it is the most well-known planetary atmosphere and its properties — such as composition, abundance and dynamics — are very well established. The atmosphere of Earth is mainly composed of $N_2$, which corresponds to a percentage of 78%, while 21% is $O_2$ and 1% is composed of gases like $CO_2$, $Ar$, water vapor, $CH_4$ and other trace gases. This composition is what provides the greenhouse effect that increases Earth's average temperature from -18°C to 15°C. $CO_2$ and water vapor are the main greenhouse gases on Earth, but there is a contribution from $CH_4$ and $N_2O$, trace gases that are almost entirely produced by life forms (Kasting and Siefert, 2002). The most evident Earth's atmospheric biosignature is $O_2$, which is mainly produced by oxygenic photosynthesis. $O_3$ (ozone) is a photolytic product of $O_2$, also considered a biomarker as it requires enough accumulation of free oxygen in the atmosphere to form (Krissansen-Totton et al., 2018).

Earth's atmosphere also shows a lot of phenomena that are essential to life. One of them is the water cycle. This molecule is not only present in the oceans, but it circulates between the surface and atmosphere, passing through the liquid, solid and vapor phases. This process causes the most noticeable atmospheric events, such as water cloud formation, rain and storms. Another phenomenon is the carbon cycle, which is essential to life due to its huge contribution to the greenhouse effect. This cycle regulates the surface temperature over large time scales and requires liquid water and plate tectonics to occur (Pont, 2014). Unlike its planetary neighbors (Venus and Mars), Earth does not have an atmosphere dominated by $CO_2$ (Lammer et al., 2018). On the contrary, the amount of carbon dioxide in its atmosphere is very small compared to other gases, representing only ∼0.04% of the atmosphere. The carbon cycle is responsible for preventing Earth from having an atmosphere dominated by $CO_2$, as it removes excess carbon dioxide from the air (Pont, 2014).

Moreover, Earth's atmosphere did not evolve from the primitive atmosphere acquired during planetary formation. According to the accretion theory of Solar System formation,

the heat produced by collisions was sufficient to vaporize all the gases that formed the first primitive atmosphere during the first million years of formation. The secondary atmosphere formed through the intense volcanic activity and lava flows that allowed the gases trapped in the planet's mantle to be released into the atmosphere. Thus, the atmosphere at that time was composed of volcanic gases and was virtually oxygen-free (Lammer et al., 2018). The advent of life, which first consisted of anaerobic microorganisms, caused the high abundance of methane about 3.8 Gyr ago. Nonetheless, the emergence of photosynthesis allowed the presence of atmospheric free oxygen on Earth. The oxygen decreased the methane abundance, as methanogenic bacteria are almost strictly anaerobic. The rise of atmospheric oxygen was the major event that built up the modern Earth's atmosphere that is seen nowadays (Kasting and Siefert, 2002; Lammer et al., 2018)

## *2.3 Mars*

Mars has an atmosphere much thinner than Earth's, with a pressure of about 6 mbar against Earth's 1 bar (Scherf and Lammer, 2021). The composition is dominated by $CO_2$, which accounts for 95.1%. The rest is composed by $N_2$ (2.8%), $Ar$ (2%) and other trace gases, like $O_2$ and $CO$ (Nier and McElroy, 1977; Trainer et al., 2019; Almatroushi et al., 2021). There is also a tiny amount of water vapor in the atmosphere. Despite the thin atmosphere, Mars contains thin water ice and $CO_2$ clouds. The low temperature and pressure on Mars allow the carbon dioxide in the air to condensate into clouds, while the small amount of water present in the atmosphere freezes (Määttänen et al., 2024).

Mars' atmosphere was formed by magma ocean outgassing, after the loss of the primordial hydrogen atmosphere during the Solar System's formation. Because Mars is about half the size of Earth and Venus, the planet was more vulnerable to the Sun's EUV flux than the other planets. It caused Mars to lose most of its steam atmosphere and remain with its current tenuous $CO_2$ atmosphere (Lammer et al., 2018; Scherf and Lammer, 2021). Also, because of its small size, Mars cooled faster than Earth, which also affected the volcanic activity and the formation of its secondary atmosphere (Lammer et al., 2018).

## 2.4 Jupiter and Saturn

Jupiter is the largest planet of the Solar System, while Saturn is the second largest. Both are gas giants that have atmospheres mainly composed of $H_2$ and $He$. Jupiter has an atmosphere composed of 86% of $H_2$ and 13.6% of $He$, while the rest is composed of minor components (e.g., $CH_4$, $NH_3$ and $H_2O$). Saturn has a similar configuration, with approximately 75-82% of $H_2$ and 18-25% of $He$. Like Jupiter, the rest of the atmosphere is composed of traces of $H_2O$, $NH_3$, $CH_4$, but also containing $PH_3$ (phosphine) (Atreya et al., 2003; Taylor et al., 2004). Besides that, Jupiter and Saturn have several cloud layers made of $H_2O$ and $NH_3$, with $NH_3$ and $H_2S$ reacting to form $NH_4HS$ clouds (Taylor et al., 2004).

The most currently accepted theory for the formation of Jupiter and Saturn states that both planets formed through core accretion. Planetesimals are accreted by collisions until they form the protoplanetary embryos. In the case of the gas giants, these embryos are massive enough to capture a large quantity of $H_2$ and $He$ from the protoplanetary disk. The gas giants grew mass enough not just to hold light molecules, but also to capture large quantities of them and evolve huge atmospheres (Pollack, 1996; Weidenschilling, 2005). They went through this process beyond the "frost line", which is the region around the star where equilibrium temperature is below 150 K and volatile molecules (such as $H_2O$, $CH_4$, $NH_3$) condense (Grasset et al., 2017). Since the components of the protoplanetary disk beyond the frost line were mainly condensed volatiles, this explains the presence of these species on these planets (Atreya et al., 2003; Pfalzner et al., 2015).

## 2.5 Neptune

Neptune is an ice giant and one of the least explored planets in the Solar System. Despite this, some observations and atmospheric models have made it possible to determine and estimate its atmospheric composition. Its atmosphere is composed mainly of 80% $H_2$ and 19% $He$, with $CH_4$ constituting about 1.5%. The planet's blue color is due, in part, to its relatively high abundance of atmospheric methane (Moses et al., 2020; Fletcher et al., 2010). Traces of hydrocarbons, such as $C_2H_6$ and $C_2H_2$, arise from the photolysis of methane in the stratosphere (Fletcher et al., 2010; Moses et al., 2020). $CO$ comes from internal and external sources (such as comet impacts), while water and $H_2S$ are found

in very low abundances in the upper atmosphere (although $H_2O$ constitutes about 27% of Neptune's total composition) (Feuchtgruber et al., 1997; Irwin et al., 2019). Most of the water is trapped in thick cloud layers, which also exist in other compositions, such as $NH_3$, $CH_4$, $H_2S$ and $NH_4HS$. Neptune's bulk composition and atmospheric abundances reflect its formation beyond the frost line, incorporating significant amounts of ices and volatile-rich planetesimals, which explain the enhanced methane and other heavy elements (Helled et al., 2020; Moses et al., 2020).

Chapter 3

# Exoplanet Atmospheres

## *3.1 Hot Jupiters*

"Hot Jupiters" (HJ) are gas giant exoplanets with short orbital periods, usually only a few days long (Fortney et al., 2021; Mansfield et al., 2021). Because of their close-in orbits, their atmospheres are subject to extremely high temperatures, strong incident radiation and they tend to be tidally locked (when there is no longer any net change in the rotation rate during the course of an orbit). These conditions create a unique atmospheric environment dominated by large day-night temperature contrasts, molecular dissociation and fast winds that can reach or even exceed the speed of sound (Fortney et al., 2021; Mansfield, 2023). They are great targets for atmospheric characterization due to their large radii and short orbital periods, which make them suitable for the transit method and thus for transmission spectroscopy (Kempton and Knutson, 2024). Because of that, the study of their atmospheres is the most advanced in exoplanet research, even though many questions regarding their nature are still unanswered.

Since there are no analogues in the Solar System, HJs challenge our intuition about planetary formation. On the one hand, Jupiter and Saturn are believed to have formed beyond the Sun's frost line, especially because, unlike terrestrial planets composed mainly of refractory material, they are rich in volatiles (Pfalzner et al., 2015). However, the detection of hundreds of hot gas giants has revealed that this is not always the rule.

There are currently three main hypotheses for the formation of HJs. The first one is "in-situ" formation, in which the hot Jupiter formed in their present-day location. The other two hypotheses claim that hot Jupiters form much further out and then migrate inwards. The process of migration might occur when there is still a gaseous disk, which generates

torques that force the planet to migrate. In the other hypothesis, migration occurs after the disk dissipation: secular interactions and planet-planet scattering put the gas giant onto a highly elliptical orbit and the planet migrates through tidal dissipation. Each one of these hypotheses leads to different HJs' properties and so the characterization of these planets can amplify our understanding about planetary formation (Fortney et al., 2021). None of the hypotheses can explain all the observational evidence, but each evidence can be explained by one of them. Despite that, the high eccentricity tidal migration might be the strongest hypothesis, as it accounts for most of the observations. The lack of small companions near hot Jupiters, the detection of eccentric hot Jupiters and the presence of distant planet companions that could lead to high eccentricity migration are evidence that support the tidal migration hypothesis. Nonetheless, tidal migration could not produce hot Jupiters with the frequency observed or account for those rare hot Jupiters with small nearby planets. Either one of the other two formation scenarios (disk migration and in-situ formation) could complement the remaining evidence that tidal migration cannot explain. Although disk migration seems to be more efficient in explaining the hot Jupiter period distribution, there is still no consensus on which one of these formation processes could be more dominant (Dawson and Johnson, 2018; Fortney et al., 2021).

Dozens of gas giant exoplanets were or are being planned to be observed with JWST (Nikolov et al., 2022). Results of atmospheric characterization through JWST observations are already published for at least 24 hot Jupiters. For these planets, the most detected molecules are $H_2O$, $CO_2$ and $CO$. Water was detected on all the planets of the sample. This is expected to occur as water is a common molecule in the universe and has strong absorption bands. While the abundance of water on Jupiter is difficult to measure from remote observations, as water is condensed in clouds in the deeper atmosphere, it is possible to obtain precise constraints on hot Jupiters. Thanks to their high temperatures, water would be in the gaseous phase occupying the observable atmosphere (Kreidberg et al., 2014), which also makes it likely detectable on these exoplanets. For the carbon-bearing species, $CO_2$ and $CO$ were detected on 14 of 24 HJs.

The atmospheres of HJs are similar to Jupiter and Saturn on a large scale. However, hot Jupiters' atmospheres are greatly affected by strong incident radiation and high temperatures. For example, HJs typically have a wide variety of atomic metals in the gas phase, like $Na$ and $K$. $CO_2$ is expected to be enhanced due to kinetic and photochemical

effects, unlike Jupiter and Saturn, which are distant from the Sun (Fortney et al., 2021). Also, $CO$ is expected to be the main carbon-bearing molecule on HJs. Other atmospheric features, like refractory clouds, were expected to be found in HJs (Fortney et al., 2021). The refractory clouds are confirmed to be present on some hot Jupiters in the sample, such as WASP-107 b and WASP-17 b. Moreover, $SO_2$ (sulfur dioxide) was also expected to be detected and was found on some exoplanets. This molecule is a consequence of photochemistry in hot Jupiters (Alderson et al., 2022; Dyrek et al., 2024).

## *3.2 Rocky planets and Sub-Neptunes*

In the Solar System, the distinction between the giant planets and the rocky planets is very clear. However, it turns out that this clear distinction does not apply to other planetary systems as expected. In fact, planets with sizes between Earth and Neptune are surprisingly abundant in our Galaxy (Wordsworth and Kreidberg, 2022). However, determining the interior composition of intermediate-density exoplanets is still not possible (Lozovsky et al., 2018). They are difficult to characterize because their densities could be consistent with various compositions, ranging from water worlds to Neptune-like compositions (Lozovsky et al., 2018; Wordsworth and Kreidberg, 2022; Kempton and Knutson, 2024). Because of that, these exoplanets usually require additional knowledge of their atmospheric properties to fully understand their interior composition. While sub-Neptunes and water worlds are more complicated to distinguish from one another without atmospheric measurements, statistical studies aim to find the transition between super-Earths and sub-Neptunes. Parc et al. (2024) found that the transition might happen at different masses and radii for each spectral type of the host star. The minimum mass for sub-Neptunes is 1.9 $M_\oplus$ for M-dwarfs, 3.4 $M_\oplus$ for K-dwarfs and 4.3 $M_\oplus$ for FG-dwarfs. Meanwhile, the maximum mass for super-Earths is the same for all spectral types: $\sim 10\ M_\oplus$. Also, density is an essential tool for distinguishing these planets (Kempton and Knutson, 2024). In the Solar System, Mars has the lowest density among the terrestrial planets ($\sim 3.9\ g/cm^3$), thus it is reasonable to consider that exoplanets with a density above this value are more likely rocky. Besides that, recent studies found that a division between super-Earths and sub-Neptunes appears to occur at $\sim 1.6\ R_\oplus$ (Lozovsky et al., 2018; Muller et al., 2024). To make a more certain classification of super-Earths and sub-Neptunes, all the criteria

mentioned above were taken into account. After separating these two types of exoplanets, we gathered results of atmospheric detections and planet properties for 20 rocky planets and 12 sub-Neptunes.

From the data, we verified that 8 rocky planets probably do not have a significant atmosphere. Other 8 planets have featureless spectra, which are devoid of atmospheric information. A featureless spectrum can be produced by a high-altitude cloud deck, a high mean-molecular-weight atmosphere or by the absence of an atmosphere (Lustig-Yaeger et al., 2023), but it is not possible to differentiate between these scenarios. Therefore, only 4 rocky planets in the sample effectively had atmospheric properties constrained. Most rocky exoplanets in the sample need more observations to constrain atmospheric properties better. JWST was expected to provide more precise observations of small exoplanets due to its larger diameter and extended infrared wavelenght range, but even with its improved capability compared to previous telescopes, there is a necessity to observe several transits of the planet to efficiently make detections and attempt to distinguish between the possible scenarios that can explain the featureless spectra (Lustig-Yaeger et al., 2023; Kirk et al., 2024; Alam et al., 2025).

Meanwhile, sub-Neptunes are more accessible to atmospheric observations than rocky exoplanets because of their extended atmospheres and larger sizes. Among the 12 sub-Neptunes, only three presented featureless spectra. Between the 9 remaining planets, $H_2O$ is the most detected molecule. $CH_4$ and $CO_2$ were detected together on 4 exoplanets and 3 exoplanets have $SO_2$ in their atmospheres, indicative of photochemistry (Beatty et al., 2024; Davenport et al., 2025). Data on sub-Neptunes is also scarce, but not for the same reason as rocky planets. In this case, atmospheres are successfully characterized by the JWST, but few planets of this type have been observed to date.

Information about the atmospheres of these exoplanets (hot Jupiters, rocky planets and sub-Neptunes) and the references used are provided in Appendix A.

Chapter 4

# Comparative Analysis

Table 4.1 shows the abundance of some molecules in exoplanets, as well as the relationship between the abundance of the exoplanet and the abundance of Jupiter and Saturn. The molecules shown are only those that hot Jupiters have in common with the Solar System (Jupiter and Saturn). Table 4.2 shows the abundance of molecules that rocky exoplanets and sub-Neptunes have in common with Earth, Venus, and Mars. In the case of sub-Neptunes, the comparison with Neptune is also shown. For some planets, the abundance was not well constrained, so they were left out of these tables.

*Table 4.1* - Comparison of molecular abundances between hot Jupiters and the Solar System

| **Planet** | **Molecules** | **Abundance (VMR)** | **Abundance Ratio** | |
|---|---|---|---|---|
| | | | **Exoplanet/Jupiter** | **Exoplanet/Saturn** |
| WASP-107 b | $H_2O$ | $(1.5^{2.2}_{0.7}) \times 10^{-4}$ | $6.5 \times 10^{-2}$ | $\sim 1.5 \times 10^{-1}$ |
| | $CH_4$ | $(1.5^{24.8}_{1.4}) \times 10^{-9}$ | $8.3 \times 10^{-7}$ | $3.3 \times 10^{-7}$ |
| | $CO_2$ | $(3.2^{196.0}_{3.2}) \times 10^{-9}$ | 8 | 11 |
| | CO | $(2.6^{4.0}_{1.9}) \times 10^{-5}$ | $3.5 \times 10^{4}$ | $2.6 \times 10^{4}$ |
| | $NH_3$ | $(9.1^{9.1}_{4.0}) \times 10^{-7}$ | $1.3 \times 10^{-3}$ | $1.5 \times 10^{-3}$ |
| | $H_2S$ | $(1.3^{2.1}_{0.7}) \times 10^{-4}$ | 1.7 | $> 6.5 \times 10^{2}$ |
| WASP-43 b | $H_2O$ | $(1.4^{5.4}_{0.8}) \times 10^{-4}$ | $5.6 \times 10^{-2}$ | $\sim 1.4 \times 10^{-1}$ |
| | $CO_2$ | $(2.5^{6.4}_{1.7}) \times 10^{-5}$ | $6.2 \times 10^{4}$ | $8.3 \times 10^{4}$ |
| | CO | $(5.6^{15.8}_{3.7}) \times 10^{-4}$ | $7.5 \times 10^{5}$ | $5.6 \times 10^{5}$ |
| | $NH_3$ | $(5.4^{10.1}_{2.7}) \times 10^{-6}$ | $7.7 \times 10^{-3}$ | $9.0 \times 10^{-3}$ |
| WASP-17 b | $H_2O$ | $(2.9^{3.9}_{1.7}) \times 10^{-5}$ | $1.2 \times 10^{-2}$ | $\sim 2.9 \times 10^{-2}$ |

*Table 4.1* - Comparison of molecular abundances between hot Jupiters and the Solar System (continued)

| Planet | Molecules | Abundance (VMR) | Abundance Ratio | |
|---|---|---|---|---|
| | | | Exoplanet/Jupiter | Exoplanet/Saturn |
| WASP-39 b | $H_2O$ | $(4.8^{1.9}_{1.4}) \times 10^{-3}$ | 1.9 | $\sim 4.8$ |
| | $CO_2$ | $(2.3^{1.2}_{0.8}) \times 10^{-4}$ | $5.8 \times 10^5$ | $7.7 \times 10^5$ |
| | CO | $(9.8^{4.3}_{3.5}) \times 10^{-3}$ | $1.3 \times 10^7$ | $9.8 \times 10^6$ |
| WASP-96 b | $H_2O$ | $(2.6^{3.2}_{1.4}) \times 10^{-4}$ | $10^{-1}$ | $\sim 2.6 \times 10^{-1}$ |
| | $CO_2$ | $(4.2^{8.1}_{3.0}) \times 10^{-5}$ | $1.1 \times 10^5$ | $1.4 \times 10^5$ |
| | CO | $(5.6^{40.0}_{5.6}) \times 10^{-4}$ | $7.5 \times 10^5$ | $5.6 \times 10^5$ |
| | $H_2S$ | — | — | — |
| WASP-77A b | $H_2O$ | $(9.5^{1.7}_{1.2}) \times 10^{-5}$ | $3.8 \times 10^{-2}$ | $\sim 9.5 \times 10^{-2}$ |
| | CO | $(1.2^{0.4}_{0.3}) \times 10^{-4}$ | $1.6 \times 10^5$ | $1.2 \times 10^5$ |
| HIP 67522 b | $H_2O$ | $(2.7^{15.0}_{2.4}) \times 10^{-4}$ | $1.1 \times 10^{-1}$ | $\sim 2.7 \times 10^{-1}$ |
| | $CO_2$ | $(2.7^{15.0}_{2.4}) \times 10^{-6}$ | $6.8 \times 10^3$ | $9.0 \times 10^3$ |
| | CO | $(1.2^{11.3}_{1.1}) \times 10^{-4}$ | $1.6 \times 10^5$ | $1.2 \times 10^5$ |
| | $H_2S$ | $(1.2^{4.3}_{1.0}) \times 10^{-5}$ | $1.6 \times 10^{-1}$ | $> 60$ |
| WASP-80 b | $H_2O$ | $(1.6^{4.7}_{1.4}) \times 10^{-2}$ | 6.4 | $\sim 16$ |
| | $CH_4$ | $(1.3^{3.8}_{1.0}) \times 10^{-4}$ | $7.2 \times 10^{-2}$ | $2.9 \times 10^{-2}$ |
| HAT-P-18 b | $H_2O$ | $(4.0^{4.0}_{2.0}) \times 10^{-5}$ | $1.6 \times 10^{-2}$ | $\sim 4.0 \times 10^{-2}$ |
| | $CO_2$ | $(1.6^{2.4}_{0.9}) \times 10^{-5}$ | $4.0 \times 10^4$ | $5.3 \times 10^4$ |
| HD 189733 b | $H_2O$ | $(2.0^{9.7}_{1.3}) \times 10^{-4}$ | $8.0 \times 10^{-2}$ | $\sim 2.0 \times 10^{-1}$ |
| | $CO_2$ | $(5.7^{21.2}_{3.6}) \times 10^{-7}$ | $1.4 \times 10^3$ | $1.9 \times 10^3$ |
| | CO | $(7.4^{48.8}_{5.4}) \times 10^{-5}$ | $9.9 \times 10^4$ | $7.4 \times 10^4$ |
| | $H_2S$ | $(3.2^{8.6}_{1.7}) \times 10^{-5}$ | $4.2 \times 10^{-1}$ | $> 1.6 \times 10^2$ |
| WASP-18 b | $H_2O$ | $(5.9^{10.7}_{2.9}) \times 10^{-4}$ | $2.4 \times 10^{-1}$ | $5.9 \times 10^{-1}$ |
| HAT-P-14 b | $H_2O$ | $(4.8^{59.8}_{4.6}) \times 10^{-3}$ | 1.9 | $\sim 4.8$ |
| WASP-94A b | $H_2O$ | $(2.6^{3.2}_{2.0}) \times 10^{-2}$ | $1.0 \times 10^1$ | $\sim 2.6 \times 10^1$ |
| | $CO_2$ | $(4.5^{10.3}_{4.5}) \times 10^{-5}$ | $1.1 \times 10^5$ | $1.5 \times 10^5$ |
| | CO | $(5.0^{12.8}_{5.0}) \times 10^{-3}$ | $6.7 \times 10^6$ | $5.0 \times 10^6$ |
| | $H_2S$ | $(2.6^{2.4}_{2.6}) \times 10^{-4}$ | 3.4 | $> 1.3 \times 10^3$ |
| WASP-15 b | $H_2O$ | $(1.5^{4.3}_{1.3}) \times 10^{-3}$ | $6.0 \times 10^{-1}$ | $\sim 1.5$ |
| | $CO_2$ | $(4.0^{17.4}_{3.6}) \times 10^{-5}$ | $1.0 \times 10^5$ | $1.3 \times 10^5$ |

*Table 4.1* - Comparison of molecular abundances between hot Jupiters and the Solar System (continued)

| Planet | Molecules | Abundance (VMR) | Abundance Ratio | |
|---|---|---|---|---|
| | | | Exoplanet/Jupiter | Exoplanet/Saturn |
| TrES-4 b | $H_2O$ | $(1.0^{4.0}_{0.8}) \times 10^{-3}$ | $4.0 \times 10^{-1}$ | $\sim 1.0$ |
| | $CO_2$ | $(1.4^{4.4}_{1.1}) \times 10^{-7}$ | $3.5 \times 10^{2}$ | $4.7 \times 10^{2}$ |
| | CO | $(1.7^{11.7}_{1.6}) \times 10^{-4}$ | $2.3 \times 10^{5}$ | $1.7 \times 10^{5}$ |
| WASP-178 b | $H_2O$ | $(5.0^{26.6}_{4.5}) \times 10^{-4}$ | $2.0 \times 10^{-1}$ | $\sim 5.0 \times 10^{-1}$ |
| | CO | $(8.9^{6.2}_{4.0}) \times 10^{-3}$ | $1.2 \times 10^{7}$ | $8.9 \times 10^{6}$ |
| TOI-5205 b | $CH_4$ | $(2.9^{1.6}_{0.9}) \times 10^{-6}$ | $1.6 \times 10^{-3}$ | $6.4 \times 10^{-4}$ |
| | $H_2S$ | $(4.8^{3.0}_{1.9}) \times 10^{-5}$ | $6.2 \times 10^{-1}$ | $2.4 \times 10^{2}$ |
| WASP-121 b | $H_2O$ | $(2.7^{1.4}_{0.8}) \times 10^{-4}$ | $1.1 \times 10^{-1}$ | $\sim 2.7 \times 10^{-1}$ |
| | CO | $(1.9^{1.8}_{1.5}) \times 10^{-3}$ | $2.5 \times 10^{6}$ | $1.9 \times 10^{6}$ |
| | $CH_4$ | $(5.6^{2.1}_{3.6}) \times 10^{-3}$ | 3.1 | 1.2 |
| WASP-19 b | $H_2O$ | $(2.8^{0.9}_{0.6}) \times 10^{-4}$ | $1.1 \times 10^{-1}$ | $\sim 2.8 \times 10^{-1}$ |
| | $CH_4$ | $(6.0^{2.3}_{1.7}) \times 10^{-6}$ | $3.3 \times 10^{-3}$ | $1.3 \times 10^{-3}$ |
| | $CO_2$ | $(8.3^{3.2}_{2.1}) \times 10^{-4}$ | $2.1 \times 10^{6}$ | $2.8 \times 10^{6}$ |
| | CO | $(1.4^{1.0}_{0.6}) \times 10^{-2}$ | $1.9 \times 10^{7}$ | $1.4 \times 10^{7}$ |

A comparative analysis of molecular abundances in hot Jupiters relative to Jupiter and Saturn reveals distinct and systematic trends among key atmospheric species. For $H_2O$, the majority of exoplanets (75%) exhibit abundances lower than Jupiter, and an equally large number also show abundances below those observed in Saturn. In contrast, carbon-bearing molecules such as carbon dioxide ($CO_2$) and carbon monoxide ($CO$) are consistently more abundant across all surveyed exoplanets when compared to both Jupiter and Saturn. Specifically, all 12 exoplanets with available measurements show $CO_2$ and $CO$ abundances between $10^4$ and $10^6$ times higher than Jupiter and Saturn. This result can be seen in Figure 4.1, which presents the ratio between the abundance of a molecule in hot Jupiters and in Jupiter as a function of the orbital period. While $H_2O$ may be relatively depleted or less enriched in hot Jupiters compared to the Solar System gas giants, $CO$ and $CO_2$ tend to be significantly enhanced. Before the launch of JWST, previous studies (Fortney et al., 2021; Mansfield et al., 2021) suggested that photochemical and kinetic processes could lead to the enhancement of $CO_2$ and $CO$ abundances in hot Jupiters. This

prediction is confirmed by JWST data available in the literature, which show how the short orbital periods of these gas giants intensify photochemistry and favor the permanence of more stable molecules, such as carbon dioxide and carbon monoxide, over molecules such as water.

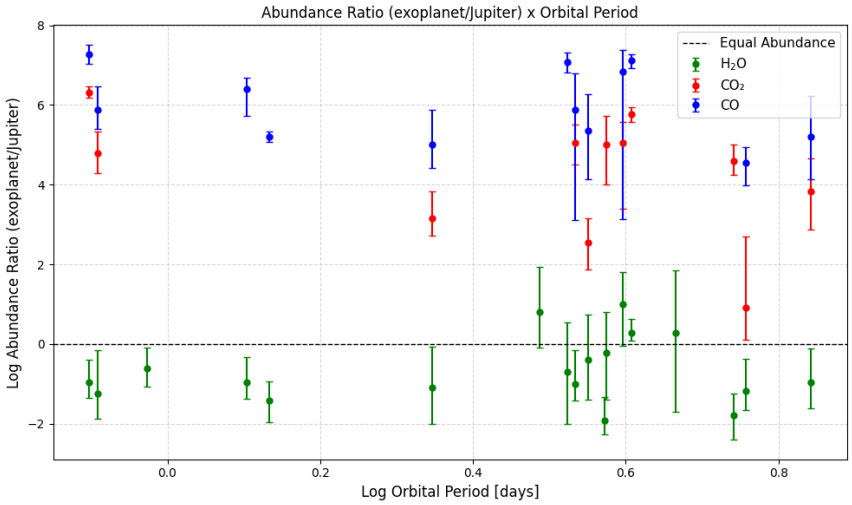


*Figure 4.1:* The ratios between the abundance in the exoplanet and in Jupiter, as a function of orbital period. Green dots are $H_2O$ abundance, red dots are $CO_2$ and blue dots are $CO$. The figure indicates that $CO_2$ and $CO$ are significantly enhanced in hot Jupiters when compared to Jupiter, while water is commonly less abundant.

The data available for rocky exoplanets observed by JWST is scarce, as the majority of them have inconclusive results or probably have no atmosphere (as mentioned before). In total, 80% of our sample composed of 20 rocky planets has inconclusive results or no atmosphere. However, when comparing these few planets to our system, we find that there is one planet for which the results are interesting from the point of view of habitability. LHS 1140 b appears to have an atmosphere mostly composed of $N_2$, as is the case on Earth. Table 4.2 contains the abundances of molecules on LHS 1140 b compared to Earth (as well as other Solar System planets). In Chapter 5, we see that this planet is also in the habitable zone, holding an equilibrium temperature of 226 K (while Earth's is around 255 K). For those reasons, this planet is the most similar to Earth, while the others are different from every Solar System rocky planet.

For sub-Neptunes, the sample of 12 exoplanets includes 3 spectra without prominent spectral bands, i.e., inconclusive results. Of the remaining nine planets, five contain $CO_2$ and four have $CH_4$ (molecules present in Neptune). Although the data is also scarce and insufficient for a reliable analysis, the comparison between abundances showed that

sub-Neptunes have $CO_2$ abundances between $10^4$ and $10^6$ times greater than Neptune. In contrast, the abundance is usually $\sim 10^2$ lower than that of Venus and slightly higher than Earth, usually between 10 and $10^2$ times higher. On the other hand, the abundance of $CH_4$ in sub-Neptunes is higher than that of Earth, but slightly lower than Neptune. In contrast, the abundance of $H_2O$ do not differ much from Neptune, except for one planet that has a thousand times less water.

The fact that sub-Neptunes have abundances of $CH_4$ and $H_2O$ that are not much different from Neptune can indicate that these exoplanets have formed in colder regions in the protoplanetary disk. At the same time, the high abundances of $CO_2$ are indicators of the presence of other chemical reactions occurring on these planets, like photochemical processes or the interaction between water and carbon. Moreover, as sub-Neptunes possess both characteristics of rocky planets and Neptune, this indicates a diversity in the atmospheres of sub-Neptunes, since they might be an intermediate case between terrestrial and gaseous planets (Bean et al., 2020).

*Table 4.2* - Comparison of molecular abundances between sub-Neptunes, rocky exoplanets and the Solar System

| Planet | Molecules | Abundance (VMR) | Abundance Ratio | | | |
|---|---|---|---|---|---|---|
| | | | Exoplanet/ Venus | Exoplanet/ Earth | Exoplanet/ Mars | Exoplanet/ Neptune |
| **Sub-Neptunes** | | | | | | |
| GJ 1214 b | $CO_2$ | $(9.1^{0.8}_{4.5}) \times 10^{-1}$ | $9.5 \times 10^{-1}$ | $2.2 \times 10^{3}$ | $9.6 \times 10^{-1}$ | $1.2 \times 10^{6}$ |
| | $CH_4$ | $(5.6^{23.9}_{5.2}) \times 10^{-3}$ | – | $3.1 \times 10^{3}$ | – | $2.8 \times 10^{-1}$ |
| K2-18 b | $CO_2$ | $(1.8^{3.2}_{1.6}) \times 10^{-2}$ | $1.9 \times 10^{-2}$ | 44 | $1.9 \times 10^{-2}$ | $2.3 \times 10^{4}$ |
| | $CH_4$ | $(7.2^{10.7}_{4.9}) \times 10^{-2}$ | – | $4.0 \times 10^{4}$ | – | 3.6 |
| | DMS | $>10^{-5}$ | – | $>1.0 \times 10^{5}$ | – | – |
| TOI-270 d | $H_2O$ | $<2.7 \times 10^{-2}$ | $<9.0 \times 10^{2}$ | 0.7–27 | <90 | $<10^{-1}$ |
| | $CO_2$ | $(1.1^{2.3}_{0.9}) \times 10^{-2}$ | $1.1 \times 10^{-2}$ | 27 | $1.2 \times 10^{-2}$ | $1.4 \times 10^{4}$ |
| | $CH_4$ | $(3.6^{4.3}_{2.4}) \times 10^{-3}$ | – | $2.0 \times 10^{3}$ | – | $1.8 \times 10^{-1}$ |
| L 98-59 d | $H_2S$ | $(2.4^{7.4}_{2.4}) \times 10^{-1}$ | – | – | – | $(0.8–2.4) \times 10^{5}$ |
| TOI-421 b | $H_2O$ | $(1.5^{30.8}_{1.2}) \times 10^{-4}$ | 5 | | $5.0 \times 10^{-1}$ | $5.6 \times 10^{-4}$ |
| | CO | $(3.8^{3711.5}_{3.8}) \times 10^{-7}$ | $9.5 \times 10^{-3}$ | $(0.04–1.5) \times 10^{-1}$ | $6.3 \times 10^{-4}$ | – |
| | | | | – | | |
| GJ 9827 d | $H_2O$ | $>3.2 \times 10^{-1}$ | $>1.1 \times 10^{4}$ | 8–320 | $>1.1 \times 10^{3}$ | >1.2 |
| GJ 3470 b | $H_2O$ | $(8.3^{14.1}_{5.8}) \times 10^{-2}$ | $2.8 \times 10^{3}$ | 2.1–83 | $2.8 \times 10^{2}$ | $3.1 \times 10^{-1}$ |
| | $CO_2$ | $(3.4^{10.4}_{2.1}) \times 10^{-3}$ | $3.5 \times 10^{-3}$ | 8.3 | $3.6 \times 10^{-3}$ | $4.4 \times 10^{3}$ |
| | $CH_4$ | $(8.9^{6.9}_{4.1}) \times 10^{-5}$ | – | 49 | – | $4.5 \times 10^{-3}$ |
| GJ 436 b | $CO_2$ | $(5.9^{263.3}_{5.9}) \times 10^{-4}$ | $6.1 \times 10^{-4}$ | 1.4 | $6.2 \times 10^{-4}$ | $7.6 \times 10^{2}$ |
| **rocky exoplanets** | | | | | | |
| 55 Cancri e | $CO_2$ | $>10^{-5}$ | $>10^{-5}$ | $>2.4 \times 10^{-2}$ | $>1.1 \times 10^{-5}$ | |
| | CO | $>10^{-2}$ | $>2.5 \times 10^{2}$ | $>10^{5}$ | >17 | |
| GJ 486 b | $H_2O$ | $>10^{-1}$ | $3.3 \times 10^{3}$ | $2.5–10^{2}$ | $3.3 \times 10^{2}$ | |
| GJ 1132 b | $H_2O$ | $(9.8^{0.2}_{6.1}) \times 10^{-1}$ | $3.3 \times 10^{4}$ | $(0.2–9.8) \times 10^{2}$ | $3.3 \times 10^{3}$ | |
| | $CH_4$ | $(4.3^{53.3}_{3.4}) \times 10^{-3}$ | – | $2.4 \times 10^{3}$ | – | |
| | $N_2O$ | $(2.3^{77.1}_{2.3}) \times 10^{-5}$ | – | 68 | – | |
| LHS 1140 b | $N_2$ | $(1.4^{8.5}_{1.4}) \times 10^{-1}$ | 4 | $1.8 \times 10^{-1}$ | 5 | |
| | $H_2O$ | $(4.6^{5.2}_{4.6}) \times 10^{-1}$ | $1.5 \times 10^{4}$ | 12–460 | $1.5 \times 10^{3}$ | |
| | $CO_2$ | $(4.8^{150.1}_{4.8}) \times 10^{-3}$ | $5.0 \times 10^{-3}$ | 12 | $5.1 \times 10^{-3}$ | |

Chapter 5

# Habitable Zone and Tidal Locking Radius

The habitable zone (HZ) was calculated using a simple algorithm based on extrapolating the solar habitable zone to other stars, using the star's luminosity and temperature as input parameters. According to Selsis et al. (2007), the inner ($R_i$) and outer ($R_o$) limits of the habitable zone of a star (given in AU) with effective temperature $T_{eff}$ and luminosity $L$ can be described by:

$$R_i = (R_{i\odot} - a_i T_* - b_i {T_*}^2)(\frac{L}{L_\odot})^{\frac{1}{2}} \tag{5.1}$$

$$R_o = (R_{o\odot} - a_o T_* - b_o {T_*}^2)(\frac{L}{L_\odot})^{\frac{1}{2}} \tag{5.2}$$

where $T_* = T_{eff} - 5700$. $R_{i\odot}$ and $R_{o\odot}$ are the limits of the Sun's habitable zone according to the criteria of Venus and Mars. The temperature is given in K and the dimensionless constants are $a_i = 2.7619 \times 10^{-5}$, $b_i = 3.8095 \times 10^{-9}$, $a_o = 1.3786 \times 10^{-4}$ and $b_o = 1.4286 \times 10^{-9}$.

The Venus criterion used to define the inner boundary of the solar HZ assumes that, at some point in its history, Venus had liquid water on its surface. Radar maps of the surface of Venus obtained during the Magellan mission show evidence that liquid water has been absent from the planet for at least 1 billion years (Solomon and Head, 1991). 1 Gyr ago, the Sun was 8% weaker, but Venus's distance from the Sun at that time provided enough solar flux to cause the water loss. For a Sun that is currently 8% stronger, the distance that corresponds to the flux received by Venus at that time is $R_{i\odot} = 0.75\ AU$. The Mars criterion, used to define the outer limit of the solar HZ, considers geological and geochemical evidence that the planet had liquid water on its surface 4 Gyr ago (Kurokawa

et al., 2014). Considering that the Sun was 28% weaker at that time, the distance that today corresponds to the same solar flux is $R_{o\odot} = 1.77\ AU$ (Selsis et al., 2007).

The values of temperatures and luminosities of the host stars used in this work were taken from the NASA exoplanet archive. The results are presented on table 5.1. Each star has a different degree of accuracy that depends on the spectral type. In general, cooler stars (type M or K) tend to have lower accuracy in measuring their temperatures and luminosities compared to hotter stars. As a result, the accuracy in calculating the habitable zone differs for each star. For simplicity, the results are given to three decimal places for all stars.

*Table 5.1* - Habitable zone boundaries.

| **System** | **Inner boundary (AU)** | **Outer boundary (AU)** |
|---|---|---|
| WASP-107 | 0.272 | 0.706 |
| WASP-43 | 0.292 | 0.767 |
| WASP-17 | 1.405 | 3.345 |
| WASP-39 | 0.630 | 1.572 |
| WASP-96 | 0.750 | 1.854 |
| WASP-77 | 0.623 | 1.536 |
| WASP-69 | 0.441 | 1.127 |
| HIP 67522 | 0.941 | 2.316 |
| HD 209458 | 0.925 | 2.240 |
| WASP-80 | 0.227 | 0.602 |
| HAT-P-18 | 0.378 | 0.966 |
| HD 189733 | 0.431 | 1.091 |
| WASP-18 | 1.153 | 2.778 |
| HD 80606 | 0.724 | 1.790 |
| WASP-52 | 0.477 | 1.207 |
| HD 149026 | 1.148 | 2.770 |
| HAT-P-14 | 1.420 | 3.401 |
| WASP-94A | 1.278 | 3.104 |
| WASP-15 | 1.174 | 2.807 |
| TrES-4 | 1.594 | 3.828 |
| WASP-178 | 2.440 | 5.446 |
| TOI-5205 | 0.106 | 0.290 |
| WASP-121 | 1.439 | 3.399 |
| WASP-19 | 0.687 | 1.695 |
| 55 Cancri | 0.582 | 1.453 |
| TRAPPIST-1 | 0.018 | 0.051 |
| GJ 486 | 0.084 | 0.231 |
| LHS 475 | 0.071 | 0.195 |
| GJ 1132 | 0.053 | 0.145 |
| LHS 1140 | 0.048 | 0.134 |
| LTT 1445A | 0.072 | 0.198 |
| L 98-59 | 0.081 | 0.221 |

*Table 5.1 continued.*

| System | Inner boundary (AU) | Outer boundary (AU) |
|---|---|---|
| GJ 341 | 0.168 | 0.449 |
| TOI-134 | 0.214 | 0.572 |
| GJ 367 | 0.129 | 0.350 |
| TOI-1685 | 0.133 | 0.363 |
| K2-22 | 0.220 | 0.585 |
| TOI-1468 | 0.097 | 0.265 |
| GJ 357 | 0.100 | 0.272 |
| TOI-836 | 0.282 | 0.737 |
| LHS 1478 | 0.064 | 0.175 |
| GJ 1214 | 0.048 | 0.132 |
| K2-18 | 0.121 | 0.328 |
| TOI-270 | 0.106 | 0.288 |
| TOI-421 | 0.537 | 1.342 |
| GJ 9827 | 0.252 | 0.661 |
| GJ 3470 | 0.144 | 0.387 |
| TOI-776 | 0.170 | 0.456 |
| GJ 3090 | 0.163 | 0.440 |
| GJ 436 | 0.116 | 0.316 |

In order to verify whether a planet is within the habitable zone, a simple algorithm was created with the semi-major axis and eccentricity of the planet's orbit as input parameters. This algorithm calculates the location of the periapsis ($R_p$) and apoasis ($R_a$) of the planet's orbit:

$$R_p = a(1 - e) \tag{5.3}$$

$$R_a = a(1 + e) \tag{5.4}$$

The values of $e$ and $a$ were also collected from the NASA exoplanet archive. With this information and the results of the inner and outer limits, we check whether the planet is entirely in the HZ, partially in the HZ (only part of its orbit passes through it) or entirely outside it.

Based on our results, only the planets K2-18 b (sub-Neptune), LHS 1140 b (rocky) and HD 80606 b (gas giant) are within the HZ, with K2-18 b and HD 80606 b being partially in it. As can be seen in Table 4.2, LHS 1140 b appears to have an atmosphere mostly composed of $N_2$, as is the case on Earth. This planet also holds an equilibrium temperature of 226 K, against Earth's 255 K. On the other hand, K2-18 b is a sub-Neptune where evidence of the molecule DMS (dimethyl sulfide) has already been detected, which

can be a biosignature under certain environmental conditions (Madhusudhan et al., 2023).

In general, stars that only host gas giants are not usually as a priority in calculating the HZ as rocky planets are. Here, we calculated the habitable zone for stars that host a single gas giant because exomoons might be of astrobiological interest. As seen in the Solar System, gas giants are planets large enough to harbor moons comparable in size to Earth. These moons may be small and cool quickly, but they may also have their own internal heat source from tidal forces between the host planet and the moon. In Jupiter and Saturn, despite being far from the solar habitable zone, the moons Europa and Enceladus are likely to have liquid water beneath their surfaces (Wandel, 2023), which opens the possibility of a biosphere. Exomoons have not yet been detected, but it is believed that, if massive enough, there is no reason to assume that they cannot be habitable (Dobos et al., 2022; Oza et al., 2019). For that reason, even though HD 80606 b is a gas giant, being in the habitable zone can bring conditions conducive to habitability on possible moons orbiting it.

The tidal locking radius is defined as the minimum distance from the star at which a planet in a circular orbit becomes tidally locked in a time $t$. According to Kasting et al. (1993), it is given by

$$r_T = 0.027(\frac{P_0 t}{Q})^{\frac{1}{6}} M^{\frac{1}{3}} \tag{5.5}$$

where $P_0$ is the original rotation period (the rotation period before orbital synchronization), $Q$ is the specific dissipation function and $M$ is the stellar mass.

Using the relation described in equation 5.5, we calculated the tidal radius for a range of stellar masses varying from 0.08 to 2 $M_\odot$ and considering three time intervals: 0.1, 1 and 10 Gyr. Since $P_0$ and $Q$ have little influence on tidal locking radius and cannot be accurately estimated, we arbitrarily chose the values $P_0 = 10\ hr$ and $Q = 100$. These values are similar to those assumed in Kasting et al. (1993). By doing this, we establish distance limits from which a planet becomes tidally locked in 0.1, 1 or 10 billion years. To verify the probability of synchronous rotation of the planets in the sample, we compared their semi-major axes and ages with the tidal radius for different times. This result is shown in Figure 5.1.

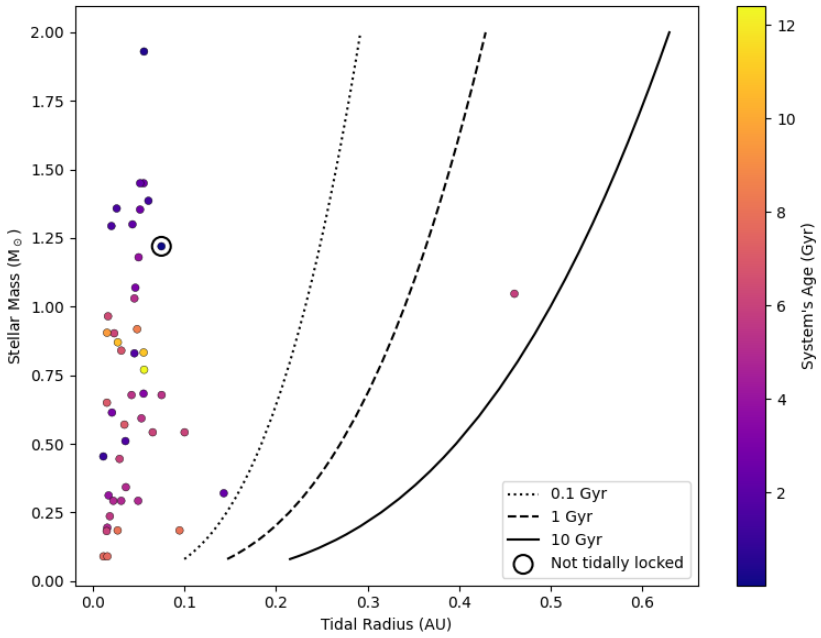


*Figure 5.1:* Stellar mass as a function of tidal locking radius for times 0.1 Gyr (dotted line), 1 Gyr (dashed line) and 10 Gyr (solid line). The color map indicates the age of the exoplanets in the sample, which are represented by dots. The only planet that is possibly not tidally locked is circled.

In Figure 5.1, planets that have a semi-major axis smaller than the tidal radius and an age greater than the time corresponding to the tidal radius are likely to be in synchronous rotation. In other words, a tidally locked planet must be located before at least one of the black lines and be old enough. We find that only one exoplanet (HIP 67522 b) is likely not yet synchronized, while all other planets are. Although this planet has the minimum distance to be synchronized, it has not had enough time to synchronize its rotation period with the orbital period. However, since its age is only 0.017 $Gyr$, it is likely to enter synchronous orbit in at most 0.083 $Gyr$.

We see that the planets found in the habitable zone, LHS 1140 b and K2-18 b, are tidally locked. This condition affects the habitability of the planets, as it causes a large temperature difference between the two hemispheres of the planet and requires the existence of an atmosphere with good heat redistribution capacity to compensate for orbital synchronization. This also affects day and night cycles, something that greatly influences life forms on Earth. In fact, habitability on tidally locked planets is still a highly debatable subject, but some studies have raised the possibility of habitable conditions existing at the terminator (i.e., the transition region between day and night) of these planets. In these regions, the temperature could be more moderate and allow for the development of life (Wandel and Gale, 2019; Wandel, 2023).

Chapter 6

# Conclusions

In this work, a bibliographic survey of atmospheric detections and abundances in exoplanets was conducted to make a comparison with the Solar System — the sample analyzed consists of 24 hot Jupiters, 20 rocky planets and 12 sub-Neptunes. For hot Jupiters, the most detected molecules are $H_2O$, $CO_2$, and $CO$, whose abundances were compared with those of Jupiter and Saturn. It was found that the abundances of $CO_2$ and $CO$ are higher in hot Jupiters than in Jupiter and Saturn, an effect that may be due to the intensification of photochemical and kinetic processes by high temperatures. The abundance of water, on the other hand, is slightly lower in hot Jupiters than in the gas giants of the Solar System.

For rocky planets, most show inconclusive results or no atmosphere, which makes the data insufficient for comparative analysis. Regarding sub-Neptunes, despite having more information, the data is also scarce and insufficient for a reliable analysis. Despite this, we found that the sub-Neptunes in the sample have abundances of $CH_4$ and $H_2O$ that do not differ much from Neptune, which may indicate that these planets formed in colder regions of the protoplanetary disk. At the same time, the high abundance of $CO_2$ relative to Neptune and Earth indicates that there are photochemical processes altering the atmosphere due to the proximity to the star. Finally, sub-Neptunes share characteristics of both rocky planets and Neptune, which proves the great diversity of these intermediate planets.

Calculations of the habitable zone and tidal locking radius showed that most of the planets in the sample are outside the habitable zone and in synchronous orbit, with the same side always facing the host star. The exceptions are the planets LHS 1140 b, K2-18 b and HD 80606 b, which are in the habitable zone and have the potential for habitability. However, they are tidally locked, since the only planet that has not yet had time to assume a synchronous orbit is HIP 67522 b, a gas giant.

Putting together all the results from the comparative analysis, habitable zone, and tidal locking radius, we see that the only planets in the habitable zone are tidally locked. LHS 1140 b, in addition to being in the habitable zone, has an atmosphere potentially similar to Earth's, that is, dominated by $N_2$ and possibly with the presence of $H_2O$ and $CO_2$, as we can see from Table 4.2. In addition, its temperature is very similar to Earth's and, despite being tidally locked, it is possible to obtain conditions conducive to life in regions close to the terminator and count on heat redistribution through the atmosphere (Wandel and Gale, 2019). The planet K2-18 b is partially in the habitable zone and tidally locked, but there have been tentative detections of a possible biosignature, DMS (a molecule that, on Earth, is only produced by phytoplankton). This planet is also a strong candidate for a hycean planet, which is a planet with an atmosphere dominated by $H_2$ and covered by oceans of water (Madhusudhan et al., 2023). HD 80606 b, despite being a gas giant, may harbor moons with the potential for habitability and could be an important target in the search for exomoons. For all these reasons, we have selected the planets LHS 1140 b, K2-18b and HD 80606 b as priority targets for future missions focused on exoplanets.

Together, these results highlight the importance of comparative atmospheric studies between different classes of exoplanets to advance our understanding of their formation trajectories, evolutionary histories and habitability. With the advent of JWST and other future observatories, increasingly accurate measurements will allow us to refine these comparisons.

# Bibliography


Alam M. K., et al., JWST COMPASS: The First Near- to Mid-infrared Transmission Spectrum of the Hot Super-Earth L 168-9 b, The Astronomical Journal, 2025, vol. 169, p. 1

Alderson L., Madhusudhan N., Apai J. M., Brogi M., Fortney J. J., Line M. R., et al. Early Release Science of the Exoplanet WASP-39b with JWST NIRSpec G395H, Nature, 2022, vol. 614

Almatroushi H., Bhardwaj A., Khayat M. M., et al. Emirates Mars Mission Characterization of Mars Atmosphere Dynamics and Processes, Space Science Reviews, 2021, vol. 217

Atreya S., Mahaffy P., Niemann H., Wong M., Owen T., Composition and origin of the atmosphere of Jupiter—an update, and implications for the extrasolar giant planets, Planetary and Space Science, 2003, vol. 51, p. 105

Bean J. L., Raymond S. N., Owen J. E., The Nature and Origins of Sub-Neptune Size Planets, Journal of Geophysical Research: Planets, 2020, vol. 126

Beatty T. G., et al., Sulfur Dioxide and Other Molecular Species in the Atmosphere of the Sub-Neptune GJ 3470 b, The Astrophysical Journal Letters, 2024, vol. 970

Davenport B., et al.,, 2025 TOI-421 b: A Hot Sub-Neptune with a Haze-Free, Low Mean Molecular Weight Atmosphere

Dawson R. I., Johnson J. A., Origins of Hot Jupiters, Annual Review of Astronomy and Astrophysics, 2018, vol. 56, p. 175

Dobos V., Haris A., Kamp I. E. E., A target list for searching for habitable exomoons, Monthly Notices of the Royal Astronomical Society, 2022, vol. 513, p. 5290

Dyrek A., et al., $SO_2$, silicate clouds, but no $CH_4$ detected in a warm Neptune, Nature, 2024, vol. 625, p. 51

Feuchtgruber H., Lellouch E., de Graauw T., et al. Detection of water vapor in Neptune's atmosphere with ISO, Nature, 1997, vol. 389, p. 159

Fletcher L. N., Orton G. S., Irwin P. G. J., et al. The AKARI infrared spectroscopy of Neptune, Astronomy  Astrophysics, 2010, vol. 514, p. A17

Fortney J. J., Dawson R. I., Komacek T. D., Hot Jupiters: Origins, structure, atmospheres, Journal of Geophysical Research: Planets, 2021, vol. 126

Grasset O., Dougherty M., Coustenis A., Witasse O., Blancquaert T., Altobelli N., Erd C., Chassefière E., Lebreton J.-P., Tiscareno M., Jaumann R., Water and Volatiles in the Outer Solar System, Space Science Reviews, 2017, vol. 212, p. 835

Helled R., Elkins-Tanton L. T., Guillot T., et al. Uranus and Neptune: Origin, Evolution and Internal Structure, Space Science Reviews, 2020, vol. 216, p. 38

Howell S. B., The Grand Challenges of Exoplanets, Frontiers in Astronomy and Space Sciences, 2020, vol. 7

Ingersoll A. P., The runaway greenhouse: A history of water on Venus, Journal of the Atmospheric Sciences, 1969, vol. 26, p. 1191

Irwin P. G. J., Fletcher L. N., Teanby N. A., et al. Detection of hydrogen sulfide above the clouds in Uranus's atmosphere, Nature Astronomy, 2019, vol. 3, p. 959

Kane S. R., Arney G., Crisp D., et al. Venus as a Laboratory for Exoplanetary Science, Journal of Geophysical Research: Planets, 2019, vol. 124, p. 2015

Kasting J. F., Siefert J. L., Life and the Evolution of Earth's Atmosphere, Science, 2002, vol. 296, p. 1066

Kasting J. F., Whitmire D., Reynolds R., Habitable zones around main sequence stars, Icarus, 1993, vol. 101, p. 108

Kempton M. R., Knutson H. A., Transiting Exoplanet Atmospheres in the Era of JWST, arXiv:2404.15430v1, 2024

Kirk J., et al., JWST/NIRCam Transmission Spectroscopy of the Nearby Sub-Earth GJ 341b, The Astronomical Journal, 2024, vol. 167

Kreidberg L., Bean J. L., Désert J. M., Benneke B., Deming D., Stevenson K. B., Berta-Thompson Z., Seifahrt A., Homeier D., A Precise Water Abundance Measurement for the Hot Jupiter WASP-43b, The Astrophysical Journal Letters, 2014, vol. 793, p. L27

Krissansen-Totton J., Bergsman D. S., Catling D. C., On Detecting Biospheres from Chemical Thermodynamic Disequilibrium in Planetary Atmospheres, Astrobiology, 2016, vol. 16, p. 39

Krissansen-Totton J., Olson S., Catling D. C., et al. Disequilibrium biosignatures over Earth history and implications for detecting exoplanet life, Science Advances, 2018, vol. 4

Kurokawa H., Sato M., Ushioda M., et al. Evolution of water reservoirs on Mars: Constraints from hydrogen isotopes in Martian meteorites, Earth and Planetary Science Letters, 2014, vol. 394, p. 179

Lammer H., Güdel M., Erkaev N., et al. Origin and evolution of the atmospheres of early Venus, Earth and Mars, The Astronomy and Astrophysics Review, 2018, vol. 26

Lozovsky M., Rogers L. A., Marcus R. A., Valencia D., Fortney J. J., Threshold Radii of Volatile-rich Planets, The Astrophysical Journal, 2018, vol. 866, p. 1

Lustig-Yaeger J., et al., A JWST transmission spectrum of the nearby Earth-sized exoplanet LHS 475 b, Nature Astronomy, 2023, vol. 7, p. 1317

Madhusudhan N., Sarkar S., Constantinou S., Holmberg M., Piette A. A. A., Moses J. I., Carbon-bearing Molecules in a Possible Hycean Atmosphere, The Astrophysical Journal Letters, 2023, vol. 956

Mansfield M., Revealing the atmospheres of highly irradiated exoplanets: from ultra hot Jupiters to rocky worlds, Astrophysics and Space Science, 2023, vol. 368

Mansfield M., Line M. R., Bean J. L., et al. A unique hot Jupiter spectral sequence with evidence for compositional diversity, Nature Astronomy, 2021, vol. 5, p. 1224

Mayor M., Queloz D., A Jupiter-mass companion to a solar-type star, Nature, 1995, vol. 378, p. 355

Moses J. I., Freedman R. S., Greathouse T. K., et al. Atmospheric chemistry on Uranus and Neptune, Philosophical Transactions of the Royal Society A, 2020, vol. 378, p. 20190477

Muller S., Guillot T., Welbanks L., Madhusudhan N., Turbet M., The mass–radius relation of exoplanets revisited, Astronomy & Astrophysics, 2024, vol. 686

Määttänen A., Lewis S. R., Wolff P. J., et al. Dust and Clouds on Mars: The View from Mars Express, Space Science Reviews, 2024, vol. 220

Nier A. O., McElroy M. B., Composition and structure of Mars' Upper atmosphere: Results from the neutral mass spectrometers on Viking 1 and 2, Journal of Geophysical Research, 1977, vol. 82

Nikolov N. K., Brogi M., Morello G., Wakeford E., Wakeford H. R., Kitzmann D., Barstow J. K., Helling C., Min M., MacDonald R. J., Schlawin E., Apai J. M., Sing D., , 2022 TrExoLiSTS: Transiting Exoplanets List of Space Telescope Spectroscopy arXiv preprint arXiv:2212.07966v1

Oza A. V., Johnson R. E., Lellouch E., Sodium and Potassium Signatures of Volcanic Satellites Orbiting Close-in Gas Giant Exoplanets, The Astrophysical Journal, 2019, vol. 885

Parc L., Marcq E., Encrenaz T., Aguichine A., Rimmer P. B., Coustenis A., From super-Earths to sub-Neptunes: Observational constraints and connections to theoretical models, Astronomy & Astrophysics, 2024, vol. 688

Pfalzner S., Davies M. B., Gounelle M., et al. The formation of the solar system, Physica Scripta, 2015, vol. 90

Pollack J. B., Formation of the Giant Planets by Concurrent Accretion of Solids and Gas, Icarus, 1996, vol. 124, p. 62

Pont F. J., Alien Skies: Planetary Atmospheres from Earth to Exoplanets. Springer, 2014

Rauer H., Catala C., Aerts C., et al. The PLATO 2.0 mission, Experimental Astronomy, 2014, vol. 38, p. 249

Scherf M., Lammer H., Did Mars Possess a Dense Atmosphere During the First Million Years?, Space Science Reviews, 2021, vol. 217

Selsis F., Kasting J. F., Levrard B., Paillet J., Habitable planets around the star Gliese 581?, Astronomy  Astrophysics, 2007, vol. 476, p. 1373

Solomon S. C., Head J. W., Fundamental issues in the geology and geophysics of venus, Science, 1991, vol. 252, p. 252

Taylor F. W., Atreya S. K., Encrenaz T., Hunten D. M., Irwin P. G. J., Owen T. C., The Composition of the Atmosphere of Jupiter, Environmental Science, Physics, 2004

Tinetti G., Drossart P., Eccleston P., et al. A chemical survey of exoplanets with ARIEL, Experimental Astronomy, 2018, vol. 46, p. 135–209

Trainer M. G., Tolbert M. A., Ghigo R. C., et al. Seasonal Variations in Atmospheric Composition as Measured in Gale Crater, Mars, Journal of Geophysical Research: Planets, 2019, vol. 121

Walker J. C. G., Evolution of the Atmosphere of Venus, Journal of the Atmospheric Sciences, 1975, vol. 32, p. 1248

Wandel A., Habitability and sub glacial liquid water on planets of M-dwarf stars, Nature Communications, 2023, vol. 14

Wandel A., Gale J., The bio-habitable zone and atmospheric properties for planets of red dwarfs, International Journal of Astrobiology, 2019, vol. 19, p. 126

Way M. J., Genio A. P. D., Aleinov J. L., et al. Was Venus the First Habitable World of Our Solar System?, Geophysical Research Letters, 2016, vol. 43, p. 8376

Weidenschilling S. J., , 2005 in Encrenaz T., Kallenbach R., Owen T. C., Sotin C., eds, Space Sciences Series of ISSI, Vol. 19, The Outer Planets and their Moons. Springer Dordrecht

Wordsworth R., Kreidberg L., Atmospheres of Rocky Exoplanets, Annual Review of Astronomy and Astrophysics, 2022, vol. 60, p. 159

# Appendix

# Appendix A

## Sample of this Work: Atmospheres and References

This appendix shows which exoplanets were selected to compose the sample, based on the criterion of having been targets of the JWST. In addition, we show the information gathered about their atmospheres, as well as the references used in the literature, in Tables A.1 (for hot Jupiters), A.2 (for rocky planets) and A.3 (for sub-Neptunes). The following tables also present information relevant to understanding the nature of these exoplanets, such as the spectral type of the host star, orbital period, mass and radius. In Chapter 3, the criteria for separating sub-Neptunes from super-Earths were explained, one of which is planetary density. In this case, the density of the planets is also shown in Tables A.2 and A.3.

*Table A.1* - Planetary properties and atmospheric detections for 24 hot Jupiters

| **Planet** | **Mass ($M_J$), Radius ($R_J$)** | **Orbital Period (days)** | **Host Star SP Type** | **Detections** | **References** |
|---|---|---|---|---|---|
| WASP-107b | 0.096, 0.94 | 5.72 | K7V | $H_2O(21\sigma), SO_2(9\sigma)$, $CH_4(5\sigma), CO_2(43\sigma), CO$ ($7\sigma$), $NH_3(6\sigma), H_2$ S($4\sigma$), silicate clouds ($7\sigma$) | NASA; Dyrek et al., 2024; Sing et al., 2024; Welbanks et al., 2024 |
| WASP-43b | 2.05, 1.00 | 0.81 | K7V | $H_2O$ ($6.5\sigma$), $NH_3(4\sigma), CO$ ($3.1\sigma$), $CO_2$ ($2.5\sigma$), nightside clouds | NASA; Yang et al., 2024; Bell et al., 2024 |
| WASP-17b | 0.51, 1.71 | 3.73 | F4V | $H_2O$ ($6.4\sigma$), $H^-(5.1\sigma)$, $SiO_2$ clouds (3.5–4.2 $\sigma$) | NASA; Gressier et al., 2025; Louie et al., 2025; Grant et al., 2023 |
| WASP-39b | 0.28, 1.36 | 4.05 | G8V | $SO_2$ ($4.8\sigma$), Na ($19\sigma$), $H_2O$ ($33\sigma$), $CO_2$ ($28.5\sigma$), CO ($7\sigma$), K ($6.8\sigma$), nongrey and inhomogeneous clouds ($\geq 8\sigma$) | NASA; Rustamkulov et al., 2023; Alderson et al., 2023; Feinstein et al., 2023; Carter et al., 2024 |
| WASP-96b | 0.48, 1.20 | 3.42 | G8V | $H_2O$ ($17\sigma$), $CO_2$ ($2.9\sigma$), CO ($2\sigma$), Na ($2\sigma$), K ($3\sigma$), $H_2$ S($2\sigma$), inhomogenous clouds and haze ($6.7\sigma$) | NASA; Radica et al., (2023); Taylor et al., 2023 |
| WASP-77Ab | 1.67, 1.23 | 1.36 | G8V | $H_2O, CO$ | NASA; August et al., 2023; Smith et al., 2024 |
| WASP-69b | 0.26, 1.06 | 3.87 | K5V | $H_2O, CO_2, CO$ | NASA; Schlawin et al., 2024 |
| HIP 67522b | 0.18–4.6, 0.89 | 6.96 | G0V | $H_2O(\geq 7\sigma), CO_2(\geq 7\sigma)$, CO ($3.5\sigma$), $H_2$ S($\approx 2\sigma$), $SO_2$ ($\approx 2\sigma$) | NASA; Thao et al., 2024 |
| HD 209458b | 0.68, 0.82 | 3.52 | G0V | $H_2O, CO_2$, clouds | NASA; Xue et al., 2024 |
| WASP-80b | 0.54, 0.95 | 3.07 | K7V | $CH_4(6.1\sigma), H_2O$ ($4.6\sigma$) | NASA; Bell et al., 2023 |
| HAT-P-18b | 0.20, 0.99 | 5.51 | K2V | $H_2O$ ($12.5\sigma$), $CO_2$ ($7.3\sigma$), He ($5.6\sigma$), uniform grey cloud deck ($7.4\sigma$), Na ($2.7\sigma$) | NASA; FournierTondreau et al., 2024; Fu et al., 2022 |
| HD 189733b | 1.17, 1.12 | 2.22 | K2V | $H_2O$ ($13.4\sigma$), $CO_2$ ($11.2\sigma$), $CO(5\sigma), H_2$ S($4.5\sigma$), $SiO_2$ clouds (6–$7\sigma$) | NASA; Fu et al., 2024; Inglis et al., 2024 |
| WASP-18 b | 10.2, 1.24 | 0.94 | F6V | $H_2O$ (>$6\sigma$), $H^-$, TiO, VO (the latter three combined $3.8\sigma$) | NASA; Coulomb et al., 2023 |
| HD 80606 b | 4.12, 1.00 | 111.44 | G8V | $CH_4$ (3.7–$4.8\sigma$), CO ($3.4\sigma$), $H_2O$ ($3.1\sigma$) | NASA; Sikora et al., 2024 |
| WASP-52 b | 0.46, 1.22 | 1.75 | K2V | $H_2O$ ($10.8\sigma$), He ($11\sigma$) with atmospheric escaping tail at $2.9\sigma$, K ($2.5\ \sigma$) | NASA; FournierTondreau et al., 2024; Kirk et al., 2022 |
| HD 149026b | 0.32, 0.81 | 2.87 | G0IV | $CO_2(3.2\sigma), H_2O$ | NASA; Bean et al., 2023 |
| HAT-P-14 b | 3.44, 1.42 | 4.63 | F5V | $H_2O(3.1\sigma)$, gray cloud deck ($1.9\sigma$) | NASA; Rongrong et al., 2025 |
| WASP-94A b | 0.50, 1.58 | 3.95 | F8V | $H_2O(\sim 4\sigma), CO_2(\sim 11\sigma)$, $CO(\sim 3\sigma)$, $H_2$ S($\sim 2.5\sigma$), cloud-covered morning limb and cloud-free evening limb ($11\sigma$) | NASA; Ahrer et al., 2025; Mukherjee et al., 2025 |
| WASP-15 b | 0.54, 1.41 | 3.75 | F7V | $H_2O(4.9\sigma), CO_2(8.9\sigma)$, $SO_2$ | NASA; Kirk et al., 2025 |
| TrES-4 b | 0.78, 1.61 | 3.55 | F8V | $H_2O(8.4\sigma), CO_2(4\sigma)$, $CO(3.1\sigma)$ | NASA; Meech et al., 2025 |
| WASP-178 b | 1.66, 1.81 | 3.34 | A1V | $H_2O, CO$ | NASA; Lothringer et al., 2025 |
| TOI-5205 b | 1.08, 1.03 | 1.63 | M4V | $CH_4(9.2\sigma), H_2S(5.2\sigma)$ | NASA; Canãs et al., 2025 |
| WASP-121 b | 1.16, 1.75 | 1.27 | F6V | $H_2O(13.5\sigma), CO(12.8\sigma), SiO(6.2\sigma), CH_4(5.1\sigma)$ | NASA; Evans-Soma et al., 2025; Gapp et al., 2025 |
| WASP-19 b | 1.15, 1.41 | 0.79 | G8V | $H_2O(16.4\sigma), CO_2(10.7\sigma), CO(5.5\sigma), CH_4(3.8\sigma), C_2H_2(2.4\sigma)$, $Al_2O_3$ clouds($2.4\sigma$) | NASA; Saha & Jenkins, 2025 |

*Table A.2* - Planetary properties and atmospheric detections for rocky exoplanets

| **Planet** | **Mass ($M_\oplus$), Radius ($R_\oplus$)** | **Orbital Period (days)** | **Density (g/cm$^3$)** | **Host Star SP Type** | **Detections** | **References** |
|---|---|---|---|---|---|---|
| 55 Cancri e | 7.99, 1.87 | 0.74 | 6.66 | K0V | $CO_2$/CO($> 3\sigma$) | NASA; Hu et al., 2024; Patel et al., 2024 |
| TRAPPIST-1 b | 1.37, 1.12 | 1.51 | 5.44 | M8V | Thin or no atmosphere | NASA; Greene et al., 2023; Ducrot et al., 2024 |
| TRAPPIST-1 c | 1.31, 1.10 | 2.42 | 5.46 | M8V | Thin or no atmosphere | NASA; Zieba et al., 2023; Radica et al., 2025 |
| GJ 486 b | 2.77, 1.29 | 1.47 | 6.66 | M3.5V | $H_2O$ ($3.6\sigma$)/stellar contamination or no atmosphere | NASA; Moran et al., 2023; Mansfield et al., 2024 |
| LHS 475 b | 0.98, 0.99 | 2.03 | 5.55 | M3.5V | Featureless spectrum | NASA; Lustig-Yaeger et al., 2023 |
| GJ 1132 b | 1.84, 1.19 | 1.63 | 5.97 | M3.5V | $H_2O$-dominated atmosphere with trace $CH_4$ and $N_2O$ or no significant atmosphere | NASA; May et al., 2023; Xue et al., 2024 |
| LHS 1140 b | 5.60, 1.73 | 23.74 | 5.90 | M4.5V | $N_2$-dominated atmosphere ($2.3\sigma$) or $N_2$ with $H_2O$ and $CO_2$ ( $3\sigma$) | NASA; Cadieux et al., 2024; Damiano et al., 2024 |
| LTT 1445A b | 2.73, 1.34 | 5.36 | 6.20 | M3V | No thick $CO_2$ atmosphere ($>4\sigma$) | NASA; Wachiraphan et al., 2024 |
| L 98-59 c | 2.25, 1.34 | 3.69 | 4.77 | M3V | Featureless spectrum | NASA; Scarsdale et al., 2024 |
| GJ 341 b | $<$4.0, 0.92 | 7.58 | - | M0V | Featureless spectrum | Kirk et al., 2024 |
| TOI-134 b | 4.07, 1.63 | 1.40 | 5.18 | M2V | Featureless spectrum | NASA; Alam et al., 2025 |
| GJ 367 b | 0.63, 0.70 | 0.32 | 10.20 | M1V | No detectable atmosphere, dark surface | NASA; Zhang et al., 2024 |
| TOI-1685 b | 3.03, 1.47 | 0.67 | 5.30 | M2V | No detectable atmosphere, dark surface | NASA; Luque et al., 2024 |
| K2-22 b | $<$445, 2.3 | 0.38 | - | K7V | Disintegrating planet, NO / $CO_2$, magnesium silicate mineral | NASA; Tusay et al., 2025 |
| TOI-1468 b | 3.04, 1.40 | 1.88 | 6.10 | M3V | No atmosphere | NASA; Valdés et al., 2025 |
| GJ 357 b | 1.84, 1.20 | 3.93 | 5.60 | M2.5V | Featureless spectrum | NASA; Taylor et al., 2025 |
| TOI-836 b | 4.53, 1.70 | 3.82 | 5.00 | K7V | Featureless spectrum | NASA; Alderson et al., 2024 |
| LHS 1140 c | 1.91, 1.27 | 3.78 | 5.10 | M4.5V | No atmosphere | NASA; Rochon et al., 2025 |
| L 98-59 b | 0.46, 0.84 | 2.25 | 4.30 | M3V | $SO_2$ atmosphere ($3.6\sigma$) | NASA; Bello-Arufe et al., 2025 |
| LHS 1478 b | 2.33, 1.24 | 1.95 | 6.70 | M3V | Inconclusive | NASA; August et al., 2025 |

*Table A.3* - Planetary properties and atmospheric detections for sub-Neptunes

| **Planet** | **Mass ($M_\oplus$), Radius ($R_\oplus$)** | **Orbital Period (days)** | **Density (g/cm$^3$)** | **Host Star SP Type** | **Detections** | **References** |
|---|---|---|---|---|---|---|
| GJ 1214 b | 8.41, 2.73 | 1.58 | 2.26 | M4.5V | $CO_2, CH_4$ (both at 3.6$\sigma$), $H_2O$ (3$\sigma$), haze | NASA; Kempton et al., 2023; Shlawin et al., 2024 |
| K2-18 b | 8.63, 2.61 | 32.94 | 2.67 | M3V | $CH_4$($\sim$ 5$\sigma$), $CO_2$ ( 3$\sigma$), DMS (<2.4$\sigma$) in a $H_2^-$ rich atmosphere | NASA; Madhusudhan et al., 2023; Schmidt et al., 2025 |
| TOI-270 d | 4.78, 2.19 | 11.38 | 2.72 | M3V | $CH_4$ (3.8–4.9$\sigma$), $CO_2$ (2.9–3.9$\sigma$), $CS_2$ (2.3–3$\sigma$), $H_2O$ (1.6–4.4$\sigma$), $C_2H_6$ (1.8–2.3$\sigma$) | NASA; Holmberg & Madhusudhan, 2024 |
| L 98-59 d | 2.14, 1.58 | 7.45 | 3.45 | M3V | $H_2S, SO_2$ (4.5$\sigma$ for both combined) | NASA; Banerjee et al., 2024; Gressier et al., 2024 |
| TOI-836 c | 9.60, 2.59 | 8.59 | 3.06 | K7V | Featureless spectrum | NASA; Wallack et al., 2024 |
| TOI-421 b | 6.70, 2.64 | 5.20 | 2.00 | G9V | $H_2O$ (4.5$\sigma$), CO (3.1$\sigma$), $SO_2$ (2.4$\sigma$), cloud- and haze-free upper atmosphere | NASA; Davenport et al., 2025 |
| GJ 9827 d | 3.02, 1.98 | 6.20 | 2.45 | K6V | $H_2O$-rich atmosphere | NASA; Piaulet-Ghorayeb et al., 2024 |
| GJ 3470 b | 12.58, 3.88 | 3.34 | 0.93 | M2V | $CO_2$ (7.3$\sigma$), $H_2O$ (6.3$\sigma$), $SO_2$ (4$\sigma$), $CH_4$ (3.8$\sigma$) | NASA; Beatty et al., 2024 |
| TOI-776 c | 5.30, 2.02 | 15.66 | 3.5 | M1V | Featureless spectrum | NASA; Teske et al., 2025 |
| TOI-776 b | 4.00, 1.85 | 8.25 | 3.4 | M1V | Featureless spectrum | NASA; Alderson et al., 2025 |
| TOI-1468 b | 3.04, 1.40 | 1.88 | 6.1 | M3V | No atmosphere | NASA; Valdés et al., 2025; Connors et al., 2025 |
| GJ 3090 b | 3.34, 2.13 | 2.85 | 1.9 | M3V | He (5.5$\sigma$) | NASA; Ahrer et al., 2025 |
| GJ 436 b | 22.1, 4.17 | 2.64 | 1.8 | M3V | $CO_2$ (2$\sigma$) | NASA; Mukherjee et al., 2025 |